Journal of
Composites Science

MDPI

Article

Synergistic Action between Copper Oxide (CuO) Nanoparticles and Anthraquinone-2-Carboxylic Acid (AQ) against *Staphylococcus aureus*

Prakhar Srivastava, Yongjun Kim, Hyejin Cho and Kwang-sun Kim *

Department of Chemistry and Chemistry Institute of Functional Materials, Pusan National University, Busan 46241, Republic of Korea
* Correspondence: kwangsun.kim@pusan.ac.kr; Tel.: +82-51-510-2241

Abstract: Infections linked to *Staphylococcus* spp. are difficult to treat with current antibiotic therapy, resulting in increased antibiotic resistance populations. One of the leading strategies to overcome this issue is the novel combination of antibacterial nanoparticles (NPs) and sustainable natural compounds. This study reported the identification of a new synergistic combination of copper oxide (CuO) NPs, a well-known antibacterial agent against *Staphylococcus* spp., and anthraquinone-2-carboxylic acid (AQ), a plant-derived antimicrobial compound, with a potent and specific fashion in killing *Staphylococcus* spp. CuO NPs were synthesized using the one-pot coprecipitation method and characterized by using X-ray diffraction and transmission electron microscopy. Further checkerboard analysis showed that CuO NPs and AQ increased the antibacterial activity of individual agents against *Staphylococcus aureus* among *Staphylococcus* spp. by four- to eightfold compared to individual materials. Additional mechanistic studies on the synergy revealed that the inhibition of biofilm formation and loss of cytoplasmic volume with cell shrinkage are the major actions of the combination in expressing the phenotype. This study clearly showed that the combination of CuO NPs and AQ would be a novel strategy to eradicate *S. aureus* infections.

Keywords: *Staphylococcus*; copper oxide; anthraquinone-2-carboxylic acid; synergy; biofilm

Citation: Srivastava, P.; Kim, Y.; Cho, H.; Kim, K.-s. Synergistic Action between Copper Oxide (CuO) Nanoparticles and Anthraquinone-2-Carboxylic Acid (AQ) against *Staphylococcus aureus*. *J. Compos. Sci.* **2023**, *7*, 135. https://doi.org/10.3390/jcs7040135

Academic Editor: Jeong-Hwan Kim

Received: 7 February 2023
Revised: 13 March 2023
Accepted: 27 March 2023
Published: 3 April 2023

1. Introduction

The most common species detected in biofilm-associated infections, such as chronic wounds and superficial skin infections, is *Staphylococcus* spp., especially *Staphylococcus aureus* (*S. aureus*) [1]. The exopolysaccharide-protected architecture of *S. aureus* allowed bacteria to congregate, increasing the metabolic activity in biofilm populations and decreasing antibiotic diffusion in the biofilm matrix [2]. The development of novel antibacterial therapies is required due to antibiotic resistance and a lack of last-resort treatments [3]. Combination therapy is routinely used to enhance the empiric coverage offered by two or more antimicrobials with different activity spectra against Gram-positive bacterial infections [4]. Furthermore, it takes advantage of avoiding or preventing resistance during single antimicrobial therapy. Due to the expanded spectrum, enhanced antibacterial activity, and reduced use of antibiotics, combination therapy has become one of the most successful ways to treat bacterial infections [5].

Metallic nanoparticles (NPs) and their oxides have been used in many different biomedical areas, including (a) inhibiting vital enzyme activity, (b) sabotaging metabolic pathways, and (c) aggregating metal ions inside bacteria [6]. Especially, inorganic NPs or oxides have been demonstrated as the most effective agents against several bacterial pathogens [7]. Among metallic NPs, copper oxide (CuO) NPs are rapidly gaining interest as they offer significant benefits in medicinal applications, such as cost-effectiveness and ease of manufacture [8]. In addition, CuO NPs have a good ion release activity compared to other noble metallic NPs, improving their solubility in medical use. According to numerous

studies, CuO NPs exhibited broad-spectrum antibacterial activity on Gram-positive and Gram-negative bacteria, such as *S. aureus*, *Bacillus* spp., *Pseudomonas aeruginosa*, *Proteus* spp., and *Escherichia coli* [9–11]. Despite their broad-spectrum action, their limitations must be overcome before being used as viable antibacterial agents, including increased minimum inhibitory concentration (MIC) values and low selectivity for various bacterial species [12,13]. Therefore, the chemical modification of CuO NPs or the combination of CuO NPs with other compounds activates CuO NPs' function at a comparable level to commercial antibiotics. Because different synthesis protocols have not improved CuO NPs' activity [14], identifying nontoxic or widely used antimicrobial compounds showing a synergistic action to CuO NPs will be a future direction to enhance the CuO NPs activity as an effective antibacterial agent against pathogens.

Several studies have reported the synergistic use of metallic NPs and their oxides with natural antimicrobial compounds or commercial antibiotics against bacterial infections. For instance, zinc oxide (ZnO) NPs in combination with commercially available antibiotics, such as ampicillin and ciprofloxacin, have increased the susceptibility pattern of *E. coli* and *S. aureus* [15]. Another study on titanium oxide (TiO_2) NPs with nalidixic acid and commercially available antibiotics (cephalosporin, β-lactam, and tetracycline) against methicillin-resistant *S. aureus* (MRSA) showed the potential synergistic activity in decreasing the susceptibility pattern of MRSA [16]. Moreover, the synergistic combination of ZnO NPs with carbapenem antibiotics has also shown potential antibiofilm and antibacterial activities against *Pseudomonas*-associated infection, highlighting the effectiveness of combination drugs against drug-resistant isolates [17]. Most studies have been conducted on silver oxide or ZnO NPs [18–20]. However, few works have been conducted on CuO NPs as a synergistic material [21]. Therefore, it is worthwhile to identify the compounds to be used as synergistic partners to CuO NPs to enhance the use of CuO NPs in a novel antibacterial therapeutic strategy against pathogens.

Natural products have been crucial to the growth of antimicrobial drugs, especially for the past 20 to 25 years [22]. These substances have been shown to affect the pathogenicity islands of bacteria, demonstrating their antibacterial potency against diseases [23]. A wide range of naturally occurring organic compounds in plants are called "plant-derived chemicals" [24]. Many studies have shown that they have beneficial antioxidant, antibacterial, and antifungal properties. An extensive family of naturally occurring substances known as anthraquinones has been demonstrated to possess antibacterial, antibiofilm, anti-inflammatory, and antioxidative activities [25–27]. Anthraquinones, such as 1,8-dihydroxyanthraquinone [28], 1-hydroxyanthraquinone [29], alizarin [30], and purpurin [31], have been shown to exhibit antibacterial and antibiofilm activities against major fungal and opportunistic bacterial pathogens. Generally, the above anthraquinones have shown an MIC of >200 μg/mL against MRSA, but emodin has better activity at an MIC of 12.5 μg/mL [32]. Moreover, emodin is known to target extracellular matrix production during early-stage biofilm development on *Staphylococcus* spp. [33,34]. Recently, anthraquinone-2-carboxylic acid (AQ) has been considered a potential biofilm inhibitor and a contender for treating *Staphylococcus*-related illnesses [32]. However, the antibacterial activity of AQ and its mechanisms have not been explored in detail, except on pathogens, such as *Clostridium* spp. [35] and *E. coli* [36]. Furthermore, the remaining question is how AQ can be used in antibacterial therapy against *Staphylococcus*.

The current market demands efficient antimicrobials targeting infectious pathogens more quickly and effectively [37]. One possible way to meet this requirement is to use drug combinations that target the same distinct pathogenicity islands of infections by antimicrobials. Like AQ, CuO NPs have been shown to prevent *S. aureus* biofilm formation [38]. Therefore, this study proposed that the synergistic interaction between CuO NPs and AQ may potentiate anti-*S. aureus* activity primarily via the biofilm architecture of *S. aureus*. Unfortunately, no report is available on the synergistic use of AQ and a nanostructured antibacterial agent, CuO NPs, to eradicate biofilm-associated infections by *Staphylococcus* spp.

This study aimed to characterize the synergistic combination of CuO NPs and AQ for increasing the antibacterial activity of CuO NPs against *Staphylococcus* spp. To this end, the synergistic potentiality of CuO NPs and AQ was performed using checkerboard analysis, and the potential action mechanisms of the combination treatment were observed by using scanning electron microscopy (SEM), biofilm formation assays, and synergy with commercially available pathway-targeted antibiotics against *Staphylococcus* spp., especially *S. aureus*. According to these findings, CuO NPs and AQ demonstrated effective synergistic efficacy by preventing biofilm development and altering cell morphology as a key mechanism. This is the first report of a synergistic combination of CuO NPs and AQ, and the combination will be used to develop an effective combination therapy for *S. aureus* infections. The novel synergistic combination of CuO NPs and AQ can be further exploited to enhance the antibacterial activity against other opportunistic pathogens.

2. Materials and Methods

2.1. Materials

CuO NPs synthesis was carried out using copper (II) chloride dihydrate ($CuCl_2{\cdot}2H_2O$; ACS reagent > 99%; Sigma-Aldrich, St. Louis, MO, USA) and sodium hydroxide (NaOH; pellets 97%; Junsei, Tokyo, Japan). The organic compound AQ ($C_{15}H_8O_4$; >99.0%) was purchased from Tokyo Chemical Industry (Tokyo, Japan). CuO NPs and AQ powder were dissolved in 1% dimethylsulfoxide (DMSO; high-performance liquid chromatography grade; Junsei).

2.2. CuO NPs Synthesis

CuO NPs were prepared using a one-pot coprecipitation process with slight modifications [14]. In a typical procedure, 0.5 M $CuCl_2.2H_2O$ and 1 M NaOH solution were prepared separately as an aqueous solution in 10 mL distilled water (dH_2O). With constant stirring, 1 M NaOH was gradually added to 0.5 M $CuCl_2{\cdot}2H_2O$, and the blue precipitate was produced instantly ($CuOH_2$; pH 10). The solution was kept at room temperature overnight with continuous stirring until the black precipitate (CuO NPs) was formed (Figure 1). The precipitate was washed thrice with ethanol and water (1:1) before being vacuum dried at 27 °C. The powdered CuO NPs was stored at room temperature until further characterization.

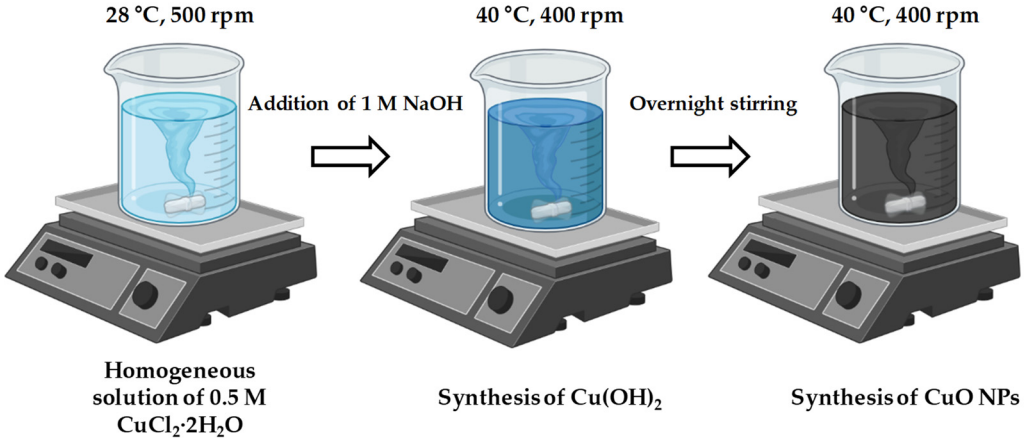

Figure 1. Schematic representation of CuO NPs synthesis.

2.3. Characterization

2.3.1. X-ray Diffraction (XRD) and Transmission Electron Microscopy (TEM)

The structure and crystallinity of CuO NPs were characterized using XRD at room temperature. Using an X-ray diffractometer (D8 Advance with the DAVINCI design; Bruker, Billerica, MA, USA) fitted with an Ni-filtered Cu Kα radiation source (1.5406 Å), the XRD pattern was captured in a 2θ range of 20° to 80°. TEM was used to assess the microstructure

of a typical CuO NPs (Bruker Nano GmbH, Berlin, Germany). The carbon-coated 300-mesh Cu grids were used to produce the TEM samples.

2.3.2. Dynamic Light Scattering (DLS) and Zeta Potential Measurement

The physical parameters of samples, such as the size and stability of NPs, were analyzed using Nanopartica SZ-100 (Horiba Ltd., Kyoto, Japan) [39,40]. The samples after the synthesis were diluted to a final concentration of 200 µg/mL using phosphate-buffered saline (PBS; pH 7; LPS Solution, Daejeon, Republic of Korea), and the temperature was maintained at 25 °C. For stability analysis, the zeta potential was measured using samples at the same concentration above either original or stored for 1 month in PBS at 4 °C after the synthesis.

2.3.3. Preparation of Bacterial Cells

Bacterial cells were obtained from the American Type Culture Collection (ATCC; Manassas, VA, USA; https://www.atcc.org; accessed on 29 March 2023) and the Korean Collection for Type Cultures (KCTC; Jeongeup, Korea; https://kctc.kribb.re.kr/; accessed on 29 March 2023). The isolates were prepared on a Luria-Bertani (LB) agar plate for 18 h at 37 °C. The Sensititre nephelometer (Thermo Fisher Scientific, Waltham, MA, USA) was used to make 0.5 McFarland turbidity bacterial suspensions.

2.3.4. MIC Determination and Checkerboard Analysis

The antibacterial activity of CuO NPs and AQ as MIC values was determined as described previously [41] using serially diluted CuO NPs and AQ solutions (31.25–1000 µg/mL) in 1% DMSO on 96-well plates (SPL, Daejeon, Republic of Korea) and bacterial suspensions in Muller–Hinton broth (MHB; MB Cells, Seoul, Republic of Korea) for 18 h at 37 °C without shaking. The fractional inhibitory concentration index (FICI) value for CuO NPs and AQ was determined as described previously [42,43]. The FICI value was calculated according to the formula: FICI = ($IC_{CuO\ NPs\ +\ AQ}/IC_{CuO\ NPs}$) + ($IC_{CuO\ NPs\ +\ AQ}/IC_{AQ}$). The interaction was considered synergistic when FICI was <0.5, additive when FICI was >0.5 to ≤1, antagonistic when FICI was ≥4, and indifferent for intermediate value.

2.3.5. Resazurin Indicator Assay

Resazurin indicator stain (7-hydroxy-3H-phenoxazin-3-one-10-oxide sodium salt, ≥95%; Sigma-Aldrich) to analyze live cells from NPs aggregates, as described previously [44]. A working concentration (0.01%) was added to each grown cell in 96-well plates, and the plates were further incubated for 3 h at 37 °C with vigorous shaking. The images were taken after bacterial growth using Samsung NX-200 (Samsung, Suwon, Republic of Korea).

2.3.6. Biofilm Formation Assay

Biofilm formation was evaluated using a plate calorimetric assay [45]. The ATCC 25923 strain was grown in LB supplemented with 0.5% glucose for 16 h at 37 °C and diluted to OD_{600} = 0.6. The culture was further diluted (1:100) in fresh LB broth, dispersed in 96-well flat-bottomed plates, mixed with samples (CuO NPs and AQ at 1/2 MIC, 1/4 MIC, 1/8 MIC, and 1/2 FICI), and incubated for 24 h at 37°C without shaking. The plates were gently washed with PBS, air dried, and subjected to 0.1% crystal violet (CV; Sigma-Aldrich) staining. Finally, the stained plates were resuspended with 30% glacial acetic acid, and the relative biofilm formation was evaluated using OD_{570}/OD_{600} values. The average ± standard deviation (SD; $p < 0.05$) were shown ($n = 7$).

2.3.7. Fluorescence Microscopy

The effects of CuO NPs and AQ on *S. aureus* biofilm architecture were examined using fluorescence microscopy with acridine orange dye (Sigma-Aldrich) [46]. In brief, overnight grown bacterial cells were diluted at 1:100 in LB broth (supplemented with 0.5% glucose)

and mixed with dH_2O, CuO NPs, AQ, and CuO NPs/AQ at specific concentrations in a six-well plate and incubated at 37 °C for 24 h under static conditions. The adhered cells were rinsed thrice with PBS and left to air dry. Acridine orange (0.01% working solution in dH_2O) was used to stain adhered cells, and the plates were then incubated at 37 °C for 10 min. After dye removal and twice PBS washes, embedded biofilm cells were examined using fluorescence microscopy (OPTIKA-B290, Ponteranica, Italy) at a ×40 objective lens.

2.3.8. Morphological Analysis of *S. aureus* ATCC 25923 with a Synergistic Combination

Morphology analysis of bacterial cells treated with CuO NPs and AQ at MIC (1000 and 125 µg/mL) and synergistic concentration (250 and 15.6 µg/mL) to overnight cultured cells were incubated for 3 h at 37 °C, 250 rpm. The culture was collected by centrifugation at 12,000 rpm for 3 min and resuspended in 500 µL PBS containing 2% formaldehyde and 1% glutaraldehyde. Cells were fixed by incubating samples for 20 min at room temperature. Further, SEM image analysis was performed as described previously [47] using VEGA3, a versatile tungsten thermionic emission SEM system (TESCAN, Fuveau, France).

2.3.9. Mechanistic Evaluation of CuO NPs and AQ with Commercially Available Antibiotics

The combinational activity of CuO NPs and AQ with available antibiotics was evaluated as described previously [48], Briefly, 5 µL CuO NPs and AQ at 1/2 MIC concentration (i.e., 500 and 62.5 µg/mL, respectively) and 1/2 synergistic value (final concentration, 125 and 7.8 µg/mL for CuO NPs and AQ, respectively) were added to 195 µL MHB inoculated with ATCC 25923 cells in a Sensititre staphylococci antibiotic susceptible plate (EUST2; Thermo Fisher Scientific). MIC was determined using the microbroth dilution method. Resazurin indicator stain was further used to differentiate NPs aggregates and grown cells.

2.3.10. Statistical Analysis

Statistical analyses for the CV assay were performed using Origin 6.1 (OriginLab, Corp., Northampton, MA, USA). Biological replicate data were presented as the average ± SD.

3. Results and Discussion

3.1. Material Properties

3.1.1. XRD Pattern

The crystalline phases of the CuO NPs sample were evaluated using XRD (Figure 2). XRD reflection peaks of the synthesized CuO NPs at 32.45°, 35.50°, 38.7°, 46.27°, 48.70°, 51.2°, 53.48°, 58.24°, 61.51°, 66.17°, 68.04°, 72.36°, and 75.09° corresponded to the (110), (002), (110), (111), (200), (112), (202), (113), (311), (022), (220), (311), and (004) planes, respectively [14]. These peaks were consistent with the crystalline CuO nanostructure (JCPDS card no- 41-0254). Hence, XRD data confirmed CuO NPs production using an easy one-pot coprecipitation approach.

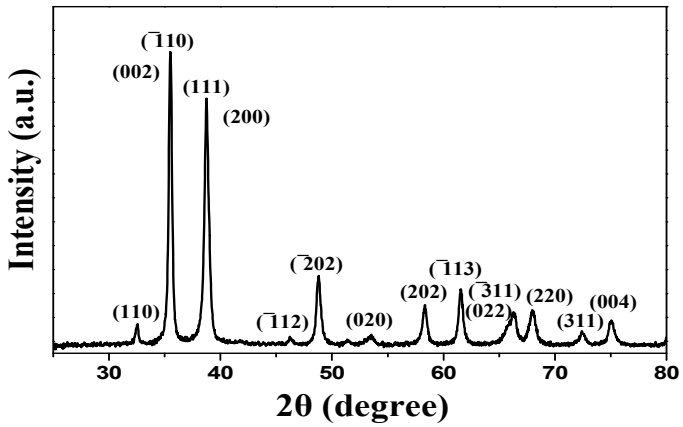

Figure 2. XRD pattern of CuO NPs.

3.1.2. Morphological Analysis

The high-resolution TEM (HR-TEM) image of the CuO NPs sample showed distinct lattice fringes with an interplanar distance of 0.27 nm (Figure 3), corresponding to the (110) plane indicated as ultrathin NPs, as described previously [49]. Hence, HR-TEM results indicated the existence of the nanoflower CuO structure, as validated by using XRD outcomes (Figure 2).

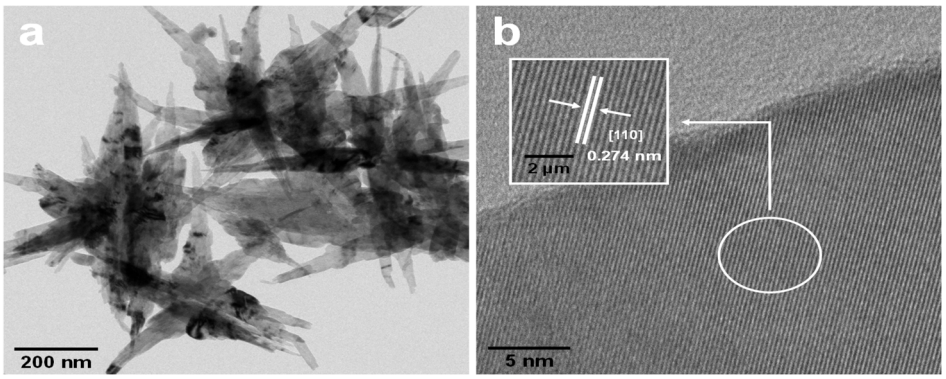

Figure 3. Morphology of CuO NPs: (**a**) TEM image and (**b**) HR-TEM image of CuO NPs.

3.1.3. Size and Stability of CuO NPs

The size of synthesized CuO NPs prepared in this study was measured using DLS. From the measurements (Figure 4a), CuO NPs were heterogeneous in size, with 84.8% of the particles in the 837 to 1967 nm range. In addition, the mean size of 1479.2 ± 456.9 nm (~1.4 µm) with maximally frequent samples was 1285 nm, suggesting that CuO NPs synthesized in this study are mainly a two-dimensional nanosheet, as characterized using TEM in a previous study [14]. Further, the stability and charge on the surface of synthesized CuO NPs were assessed by using zeta potential analysis [50], which measures the magnitude of the repulsion or attraction between particles. The surface potential of NPs is responsible for the behavior of colloidal NPs in aqueous solutions due to their ionic characteristics. The mean zeta potential values of CuO NPs either after the original (after the synthesis) or its storage in PBS at 4°C for 1 month were 38.3 ± 0.72 and 36.8 ± 1.31 mV, respectively, which deviated by <4% (Figure 4b), indicating that synthesized CuO NPs are stable cationic materials.

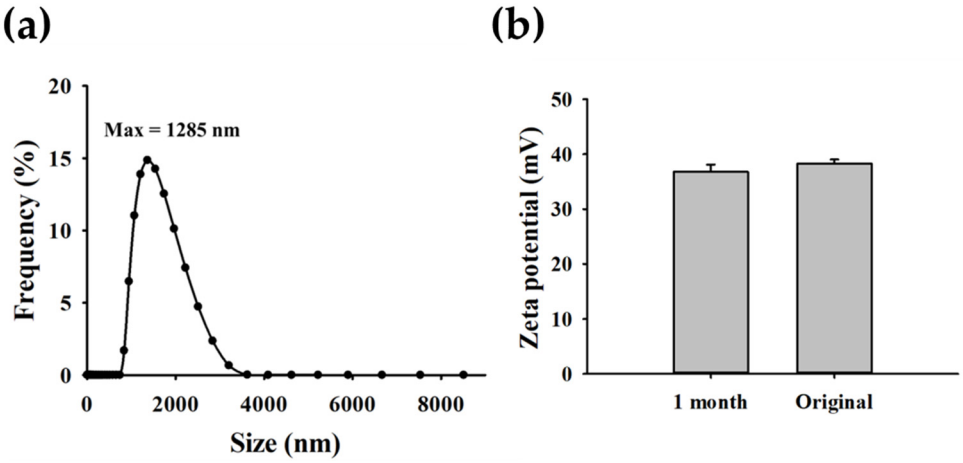

Figure 4. Measurement of the (**a**) zeta potential and (**b**) size of CuO NPs. The zeta potential of both original samples from the synthesis and 1 month after synthesis was measured. Data are shown as the mean ± SD ($n = 3$; $p < 0.05$).

3.2. Antibacterial Activity

3.2.1. Evaluation of Antibacterial Activity

The MIC of CuO NPs and AQ against the *S. aureus* (ATCC 25923) strain was determined using a 96-well plate broth microdilution method, corroborating with the resazurin viability assay. In Figure 5, the MIC values of AQ and CuO NPs against ATCC 25923 were 125 and 1000 µg/mL, respectively. The efficacy of CuO NPs and AQ to two MRSA strains is shown in Table 1. Results showed that the MIC of AQ against MRSA1 (Figure S1b) and MRSA2 (Figure S1c) was 250 µg/mL (Figure S1b,c), indicating that the antibacterial activity of AQ against MDR strains was less effective than that of the non-MDR *S. aureus* strain. Next, the antibacterial activity of AQ and CuO NPs against other *Staphylococcus* spp. was evaluated to see the selectivity of both materials. To this end, *Staphylococcus epidermidis* (Figure S1d,e) and *Staphylococcus saprophyticus* (Figure S1f), which reside together with *S. aureus* as common skin pathogens [51], were selected, and the MIC of both materials was determined. Results showed that CuO NPs against all Staphylococcus strains showed the same activity (MIC = 1000 µg/mL; Table 1).

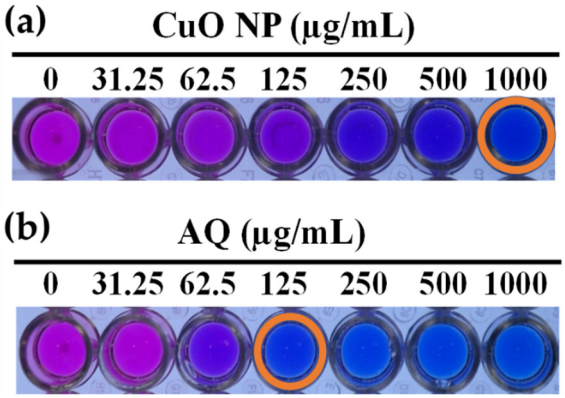

Figure 5. MIC of (**a**) CuO NPs and (**b**) AQ incubated against the *S. aureus* (ATCC 25923) strain at 37 °C for 18 h. The resazurin plate images were captured using a digital NX-200 camera (Samsung). One of the representatives is shown (n = 3). Orange circles indicate MIC values.

Table 1. MIC of CuO NPs and AQ against *Staphylococcus* strains.

Species	Strain Type	Strain Number	MIC (µg/mL)	
			CuO NPs	AQ
S. aureus	Type	ATCC 25923	1000	125
	MDR	MRSA1	1000	250
	MDR	MRSA2	1000	250
S. epidermidis	Type	KCTC 13171	1000	125
	MSSE	ATCC 12228	500	62.5
S. saprophyticus	Type	ATCC 15305	1000	250

Detailed strain information is provided in a previous report [47,48]. MSSE, methicillin-susceptible *S. epidermidis*.

Meanwhile, AQ against type strains of *S. epidermidis* (KCTC 13171; Figure S1d) and *S. saprophyticus* (ATCC 15305; Figure S1f) is the same activity (MIC = 125 µg/mL) as *S. aureus*, whereas AQ in *S. saprophyticus* is twofold less active (MIC = 250 µg/mL) than *S. aureus* and *S. epidermidis*. The above data indicated *that S. aureus* and *S. epidermidis* are better targets for the synergistic action between CuO NPs and AQ. Furthermore, the effects of MDR *S. aureus* and *S. epidermidis* were assessed on CuO NPs and AQ. In Table 1, CuO NPs and AQ against MDR *S. epidermidis* showed twofold more activity (MIC = 62.5 µg/mL) than type strain, whereas AQ was less active to MDR *S. aureus*. These findings suggested that AQ shows a preference for MDR *S. epidermidis*, a commensal pathogen that does not

produce enterotoxins, unlike *S. aureus* [52]. Comparatively, the clinical type of *S. epidermidis* (Figure S1e) is less virulent; therefore, it is less prominent in antibiotic resistance and easily targeted by potential antimicrobial agents [53].

3.2.2. Checkerboard Analysis of CuO NPs/AQ Combination against *S. aureus*

In Table 1, *S. aureus* (MRSA1 and MRSA2), *S. epidermidis* (ATCC 12228), and *S. saprophyticus* ATCC 15305 were also tested for the synergistic action of CuO NPs with AQ by checkerboard analysis. However, the FICI value was >0.5 (Table 2). Of all these isolates, *S. aureus* ATCC 25923 showed good synergy based on FICI values and was taken further for the subsequent work. Figure 6 highlights the four- or eightfold increased antibacterial activity of CuO NPs AQ by MIC. The FICI at the visible MIC of the combination between CuO NPs (250 µg/mL) and AQ (15.6 µg/mL) was 0.375, clearly showing the synergistic activity of CuO NPs and AQ.

Table 2. MIC and FICI values of CuO NPs, AQ, and their combination against *Staphylococcus* spp.

Species	Strain Type	Strain ID	Single Component		Combination		FICI
			MIC (µg/mL)				
			CuO NPs	AQ	CuO NPs	AQ	
S. aureus	Type	ATCC 25923	1000	125	250	15.6	0.37
	MDR	MRSA1	1000	250	250	125	0.75
	MDR	MRSA2	1000	250	500	62.5	0.75
S. epidermidis	Type	KCTC 13171	1000	125	250	62.5	0.75
	MSSE	ATCC 12228	500	62.5	250	15.6	0.75
S. saprophyticus	Type	ATCC 15305	1000	250	500	125	1

Detailed strain information is provided in a previous report [47,48].

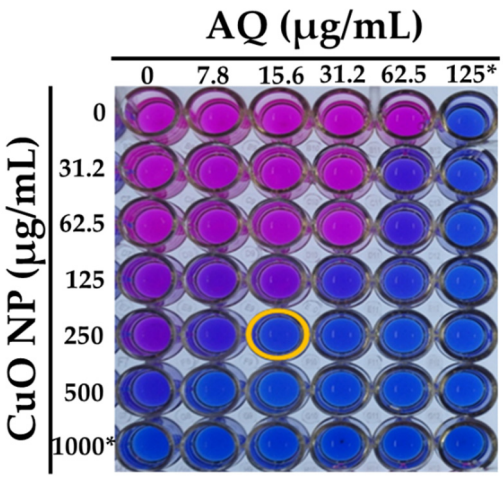

Figure 6. Checkerboard analysis of CuO NPs and AQ against ATCC 25923 with resazurin dye. The 96-well plate was imaged with a digital camera (Samsung NX200). The asterisk represents MIC, and the orange circle indicates the position FICI = 0.375.

3.3. Plausible Antibacterial Mechanism

3.3.1. Biofilm Inhibition Assay

ATCC 25923 is a widely studied *S. aureus* strain to evaluate antibacterial and biofilm formation [54]. Biofilm formation is a potential factor that acts as a barrier against vari-

ous antimicrobial agents and modifies the susceptibility pattern of *S. aureus* [55]. In the checkerboard assay (Figure 6), the antibacterial activity of individual CuO NPs and AQ was reduced against ATCC 25923. Because AQ and CuO NPs are correlated to antibiofilm activity [32,38], this combination will reduce the ability of *S. aureus* to form a biofilm structure. Moreover, a previous study on CuO NPs [56] and plant-derived anthraquinones, such as rhein and emodin, have shown potent antibiofilm activity against various Gram-negative and Gram-positive pathogens [57,58]. However, the synergistic role of AQ with a potential antibacterial metallic NPs counterpart has not been characterized. To verify this hypothesis, a CV assay was performed with the ATCC 25923 strain using CuO NPs, AQ, and CuO NPs/AQ synergistic combination. Results showed that individual CuO NPs and AQ inhibited the biofilm formation of ATCC 25923 in a dose-dependent manner, and the better ability of AQ in this action (Figures 7a and S2). As expected, the inhibition activity of biofilm formation by a $\frac{1}{2}$ synergistic concentration of CuO NPs and AQ (125 and 7.8 µg/mL, respectively) was stronger than those of individual materials. Quantitatively, CuO NPs at 1/8 MIC and AQ at 1/16 MIC inhibited 27% and 19% of biofilm inhibition, whereas the synergistic combination inhibited the biofilm formation of *S. aureus* by >80%. This highlighted that the antibiofilm activity of synergistic combination is a major antibacterial action mechanism.

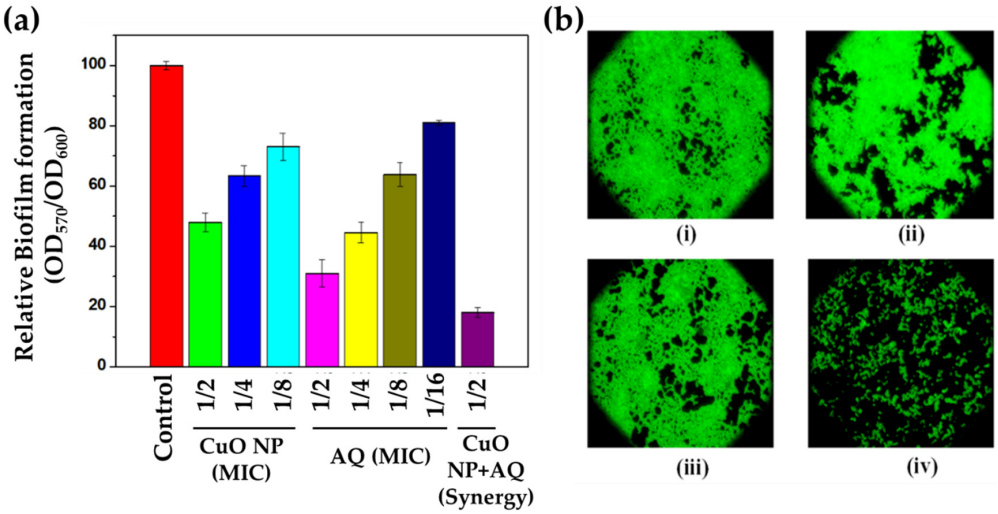

Figure 7. Effects of synergy on biofilm formation. (**a**) Relative biofilm formation (OD_{570}/OD_{600}) was determined for *S. aureus* (ATCC 25923) cells under the absence or presence of samples at MIC or half of the synergistic level. C, control; CuO NPs (1/2, 1/4, or 1/8 MIC)]; AQ (1/2, 1/4, 1/8, or 1/16 MIC); CuO NPs/AQ (1/2 synergy)]. The values in the graph represent the average ± SD (n = 7). (**b**) Microscopic analysis of biofilm architecture of *S. aureus* ATCC 25923 cells. (**i**) Control, (**ii**) CuO NPs (1/8 MIC), (**iii**) AQ (1/16 MIC), and (**iv**) CuO NPs/AQ (1/2 synergy).

In addition to CV-based biofilm inhibition experiments (Figures 7a and S2), fluorescence microscopy analysis was conducted to examine the biofilm architecture of live cells because CV analysis often reflects the mixture of biofilm mass from live and dead cells [34,59]. In Figure 7b, the population of live bacterial biofilm cells after treatment of CuO NPs 1/8 or AQ 1/16 MIC was discernable compared to the control, whereas CuO NPs/AQ at 1/2 synergistic concentration displayed ~81% decrease in the total biofilm cells. Additional SEM image analysis confirmed the decreased number of live biofilm cells in the CuO NPs/AQ combination (Figure S3). All the above data demonstrated that the enhanced killing effect of CuO NPs/AQ against *S. aureus* is associated with biofilm architecture.

3.3.2. Morphological Characterization of Cells: Cell Shrinkage and Loss of Cytoplasmic Volume

The synergistic combination potentiates the antibacterial activity against *S. aureus* and predominately affects the biofilm mode of its growth (Figure 7). In general, the

antibacterial activity of NPs involves membrane disruption. Therefore, the direct evidence of morphological changes or damage by synergistic materials as an additional mechanism of action needs to be investigated. To this end, SEM image analysis was performed to evaluate the physical and morphological changes in bacterial cells by the synergistic combination. In Figure 8a, ATCC 25923 cells without treating CuO NPs and/or AQ did not change their compact morphology. However, the treatment of CuO NPs or AQ at the MIC level, even for a short time, induced the irregularity and heterogeneous morphology of the cells (Figure 8b,c). This morphology was much stronger in synergistic conditions, where the severely shrunken structure of cell walls with many scars is shown (Figure 8d), confirming that cell wall deformation through the loss of cytoplasmic volume of cells by the CuO NPs/AQ synergy would enhance cell wall deformation, as shown in graphene oxides [60]. The above results and a previous report suggested a schematic model for the action of CuO NPs/AQ synergistic combination against *S. aureus* (Figure 9). A similar model is well known in xerotolerant bacteria, extremophiles that can survive in environments with extremely limited water availability [61]. Therefore, CuO NPs/AQ seems to make the desiccated status of *S. aureus*.

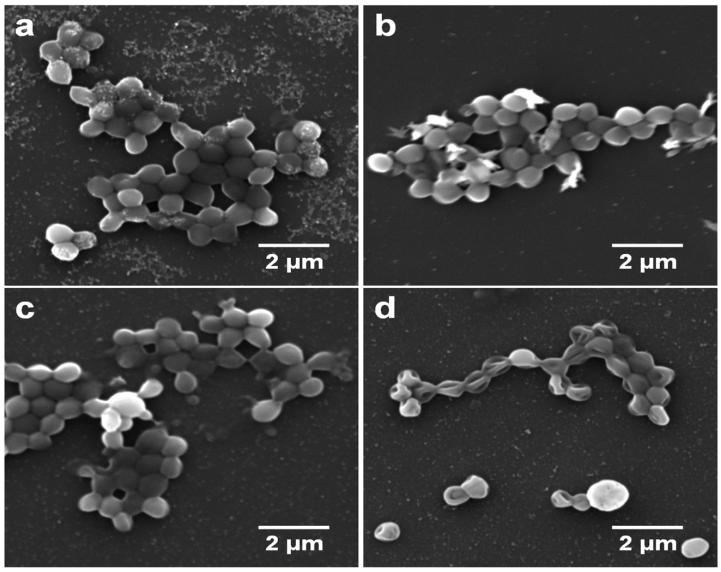

Figure 8. Morphology changes by CuO NPs and AQ. SEM images of *S. aureus* ATCC 25923 cells: (**a**) control, (**b**) CuO NPs (MIC), (**c**) AQs (MIC), and (**d**) CuO NPs/AQ at the synergistic level. Overnight grown cells were treated for 3 h with samples and imaged. One of the representatives is shown (n = 3).

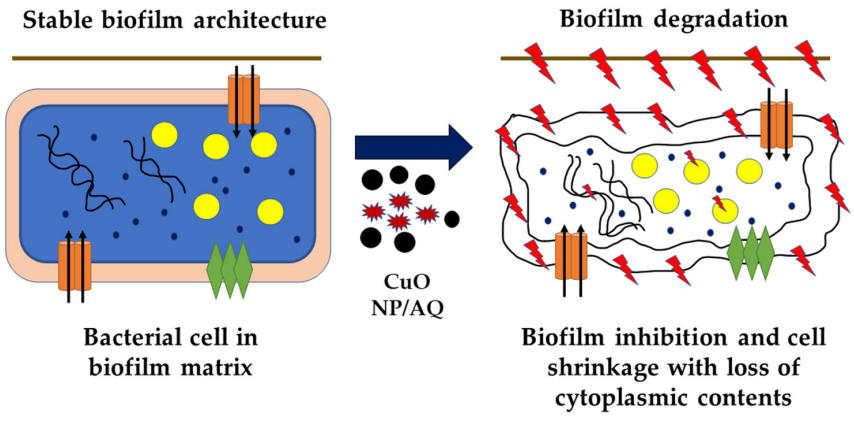

Figure 9. Schematic representation of CuO NPs/AQ combination action on the morphology of *S. aureus* cells.

3.3.3. Mechanistic Behavior of the Synergistic Combination with Antibiotics

To understand the intrinsic factors or pathways involved in the synergistic combination of CuO NPs and AQ, screenings of synergistic antibiotics of known mechanisms for CuO NPs/AQ combination were performed. To this end, the MIC values for individual antibiotics by CuO NPs, AQ, or both at the sub-MIC level of CuO NPs (500 μg/mL), AQ (62.5 μg/mL), and CuO NPs/AQ (1/2 synergy; 125 and 7.8 μg/mL for CuO NPs and AQ, respectively) against ATCC 25923 cells were determined using a premade MIC plate for Gram-positive bacteria, coated with different concentrations of 19 commercial antibiotics or combinations. From the screenings (Table 3), only gentamicin (GEN) and streptomycin (STR) showed increased antibacterial activity by the synergy of CuO NPs and AQ with more than twofold, in which MIC was changed from 0.25 to <0.12 μg/mL for GEN and 2 to <1 μg/mL for STR to the control (Figure S4). To identify the origin of synergistic action, the MIC of GEN and STR was determined under CuO NPs or AQ at the 1/2 MIC level. When the MIC of GEN and STR was compared to the control and synergy samples, CuO NPs made cells more susceptible to both antibiotics, whereas that treated with AQ was reduced. Based on the inhibitory mechanism of GEN and STR, the increased susceptibility of GEN and STR against *S. aureus*, mainly by CuO NPs, is the inhibition of the protein synthesis pathway [62,63]. Therefore, the synergistic combination of CuO NPs and AQ might create cell shrinkage from within (Figure 6) rather than the modulation of intracellular pathways.

Table 3. Screening of antibiotics modulated by CuO NPs, AQ, or their synergy.

Antibiotics	Acronym	MIC [1] (μg/mL)			
		Control	+CuO NPs	+AQ	Synergy
Kanamycin	KAN	<1	<1	<1	<1
Streptomycin	STR	2	<1	4	<1
Tiamulin	TIA	0.5	0.5	0.5	0.5
Quinupristin/dalfopristin	SYN	0.25	1	0.25	0.5
Linezolid	LZD	2	2	2	2
Mupirocin	MUP	<0.12	<0.12	<0.12	<0.12
Vancomycin	VAN	1	2	1	1
Chloramphenicol	CHL	8	8	8	8
Fusidic acid	FUS	0.25	0.25	0.5	0.5
Penicillin	PEN	0.06	0.12	0.06	0.12
Trimethoprim	TMP	>4	>4	2	>4
Rifampin	RIF	0.008	<0.008	0.015	0.008
Erythromycin	ERY	0.25	0.25	0.25	0.25
Ciprofloxacin	CIP	0.12	0.12	0.25	0.25
Tetracycline	TET	0.25	0.5	0.25	0.5
Clindamycin	CLI	0.12	0.12	0.06	0.12
Cefoxitin	FOX	2	1	2	2
Gentamicin	GEN	0.25	0.12	0.25	<0.12
Sulfamethoxazole	SMX	32	128	>128	>128

[1] The MIC values were determined using the Sensititre Staphylococci antibiotic-susceptible plate (EUST2; Thermo Fisher Scientific) with a total volume of 200 μL. Red indicates the increase in the fold change compared to the control set. Reproducible data are shown ($n > 3$). The concentrations used for the screening were at 1/2 MIC: CuO NPs and AQ at 500 or 62.5 μg/mL, respectively, in evaluating single material with antibiotics, whereas those in the synergy were used either 125 or 7.8 μg/mL, respectively.

4. Limitations and Perspectives

CuO NPs have been suggested as a potential synergistic material in medical healthcare systems. However, its high MIC and low selectiveness against pathogens limit its use as a biocompatible antibacterial agent. In particular, the high dosage of CuO NPs against target hosts increases the chances of cell cytotoxicity, resulting in increased oxidative damage, inhibition of antioxidant pathways, chromosomal aberrations, and DNA damage. Generally, the route of synthesis, crystallographic appearance, and chemical composition affect the function of antibacterial NPs. However, CuO NPs with desired morphologies prepared

with the help of physical and chemical stimuli, such as high temperature, pressure, longer reaction time, and use of different chemical reagents, have not resolved the limitation. Still, it is possible that surface modification involving chemical stability, surface reactivity, nanofabrication with capping agents, dissolution factor, and effective exposure route will enhance the biocompatible effectivity of CuO NPs, which needs to be studied further.

5. Conclusions

In this study, CuO NPs and AQ could be a selective synergistic combination against *S. aureus* among other *Staphylococcus* spp. From mechanistic studies, the combination can potentiate the antibacterial activity mainly by cell disruption and decreased biofilm formation. This study highlighted the potential effects of the synergistic combination in reducing live biofilm-forming cells. This is an additional advantage in using these combinations against recurrent infection models, such as chronic nonhealing wounds, which display a biofilm-forming cell-associated reduction in antimicrobial activity. Synergistic actions of metallic NPs with natural compounds have been reported, but the one that potentiates activity and selectiveness by CuO NPs has not been characterized. To the authors' knowledge, this is the first study that showed the induced antibacterial capability of CuO NPs with the combination of AQ and their possible action mechanisms against *S. aureus*. Therefore, all information can be used in the appropriate formulation of prospective synergistic candidates that could significantly boost the use of natural antimicrobials against *S. aureus*.

Supplementary Materials: The following supporting information can be downloaded at: https://www.mdpi.com/article/10.3390/jcs7040135/s1, Figure S1: Broth microdilution analysis using resazurin based assay against *S. aureus*.; Figure S2: Image of Crystal violet assay.; Figure S3: SEM analysis of *S. aureus* (ATCC 25923) biofilm architecture.; Figure S4: Screening of synergistic antibiotics with CuO NP, AQ, and CuO NP/AQ.

Author Contributions: P.S. and K.-s.K. designed the experiments. P.S., Y.K., and H.C. carried out the experiments. P.S. and K.-s.K. wrote the original manuscript. K.-s.K. supervised the research and revised the original manuscript. All authors have read and agreed to the published version of the manuscript.

Funding: This research was funded by a National Research Foundation of Korea (NRF) grant funded by the Korean government (MSIT) (grant number NRF-2021R1A2C1007413).

Institutional Review Board Statement: Not applicable.

Data Availability Statement: Not applicable.

Acknowledgments: We would like to thank the Korean Collection for Type Cultures (KCTC) for providing the pathogens (KCTC No. 13171) used in this study. Figure 1 and graphical abstract were prepared by BioRender (www.biorender.com; accessed on 13 March 2023).

Conflicts of Interest: The authors declare that they have no known competing financial interest or personal relationships that could have appeared to influence the work reported in this paper.

References

1. Roy, S.; Santra, S.; Das, A.; Dixith, S.; Sinha, M.; Ghatak, S.; Ghosh, N.; Banerjee, P.; Khanna, S.; Mathew-Steiner, S.; et al. *Staphylococcus aureus* Biofilm Infection Compromises Wound Healing by Causing Deficiencies in Granulation Tissue Collagen. *Ann. Surg.* **2020**, *271*, 1174–1185. [CrossRef] [PubMed]
2. Aguila-Arcos, S.; Alvarez-Rodriguez, I.; Garaiyurrebaso, O.; Garbisu, C.; Grohmann, E.; Alkorta, I. Biofilm-Forming Clinical *Staphylococcus* Isolates Harbor Horizontal Transfer and Antibiotic Resistance Genes. *Front. Microbiol.* **2017**, *8*, 2018. [CrossRef] [PubMed]
3. Leon-Buitimea, A.; Garza-Cardenas, C.R.; Garza-Cervantes, J.A.; Lerma-Escalera, J.A.; Morones-Ramirez, J.R. The Demand for New Antibiotics: Antimicrobial Peptides, Nanoparticles, and Combinatorial Therapies as Future Strategies in Antibacterial Agent Design. *Front. Microbiol.* **2020**, *11*, 1669. [CrossRef] [PubMed]
4. FakhriRavari, A.; Simiyu, B.; Morrisette, T.; Dayo, Y.; Abdul-Mutakabbir, J.C. Infectious disease: How to manage Gram-positive and Gram-negative pathogen conundrums with dual beta-lactam therapy. *Drugs Context* **2022**, *11*, 2021–8–9. [CrossRef] [PubMed]

5. Grillo, S.; Puig-Asensio, M.; Schweizer, M.L.; Cuervo, G.; Oriol, I.; Pujol, M.; Carratala, J. The Effectiveness of Combination Therapy for Treating Methicillin-Susceptible *Staphylococcus aureus* Bacteremia: A Systematic Literature Review and a Meta-Analysis. *Microorganisms* **2022**, *10*, 848. [CrossRef] [PubMed]
6. Slavin, Y.N.; Asnis, J.; Hafeli, U.O.; Bach, H. Metal nanoparticles: Understanding the mechanisms behind antibacterial activity. *J. Nanobiotechnol.* **2017**, *15*, 65. [CrossRef] [PubMed]
7. Abo-Shama, U.H.; El-Gendy, H.; Mousa, W.S.; Hamouda, R.A.; Yousuf, W.E.; Hetta, H.F.; Abdeen, E.E. Synergistic and Antagonistic Effects of Metal Nanoparticles in Combination with Antibiotics Against Some Reference Strains of Pathogenic Microorganisms. *Infect. Drug Resist.* **2020**, *13*, 351–362. [CrossRef]
8. Ermini, M.L.; Voliani, V. Antimicrobial Nano-Agents: The Copper Age. *ACS Nano* **2021**, *15*, 6008–6029. [CrossRef]
9. Xiao, J.; Zhu, Y.; Huddleston, S.; Li, P.; Xiao, B.; Farha, O.K.; Ameer, G.A. Copper Metal-Organic Framework Nanoparticles Stabilized with Folic Acid Improve Wound Healing in Diabetes. *ACS Nano* **2018**, *12*, 1023–1032. [CrossRef]
10. Guo, J.; Gao, S.H.; Lu, J.; Bond, P.L.; Verstraete, W.; Yuan, Z. Copper Oxide Nanoparticles Induce Lysogenic Bacteriophage and Metal-Resistance Genes in *Pseudomonas aeruginosa* PAO1. *ACS Appl. Mater. Interfaces* **2017**, *9*, 22298–22307. [CrossRef]
11. Laha, D.; Pramanik, A.; Laskar, A.; Jana, M.; Pramanik, P.; Karmakar, P. Shape-dependent bactericidal activity of copper oxide nanoparticle mediated by DNA and membrane damage. *Mater. Res. Bull.* **2014**, *59*, 185–191. [CrossRef]
12. Das, D.; Nath, B.C.; Phukon, P.; Dolui, S.K. Synthesis and evaluation of antioxidant and antibacterial behavior of CuO nanoparticles. *Colloids Surf B Biointerfaces* **2013**, *101*, 430–433. [CrossRef] [PubMed]
13. Moniri Javadhesari, S.; Alipour, S.; Mohammadnejad, S.; Akbarpour, M.R. Antibacterial activity of ultra-small copper oxide (II) nanoparticles synthesized by mechanochemical processing against *S. aureus* and *E. coli*. *Mater. Sci. Eng. C Mater. Biol. Appl.* **2019**, *105*, 110011. [CrossRef] [PubMed]
14. Ghosh, A.; Miah, M.; Bera, A.; Saha, S.K.; Ghosh, B. Synthesis of freestanding 2D CuO nanosheets at room temperature through a simple surfactant free co-precipitation process and its application as electrode material in supercapacitors. *J. Alloys Compd.* **2021**, *862*. [CrossRef]
15. Banoee, M.; Seif, S.; Nazari, Z.E.; Jafari-Fesharaki, P.; Shahverdi, H.R.; Moballegh, A.; Moghaddam, K.M.; Shahverdi, A.R. ZnO nanoparticles enhanced antibacterial activity of ciprofloxacin against *Staphylococcus aureus* and *Escherichia coli*. *J. Biomed. Mater. Res. B Appl. Biomater.* **2010**, *93*, 557–561. [CrossRef]
16. Roy, A.S.; Parveen, A.; Koppalkar, A.R.; Prasad, M.V.N.A. Effect of Nano-Titanium Dioxide with Different Antibiotics against Methicillin-Resistant *Staphylococcus aureus*. *J. Biomater. Nanobiotechnol.* **2010**, *1*, 37–41. [CrossRef]
17. El-Telbany, M.; Mohamed, A.A.; Yahya, G.; Abdelghafar, A.; Abdel-Halim, M.S.; Saber, S.; Alfaleh, M.A.; Mohamed, A.H.; Abdelrahman, F.; Fathey, H.A.; et al. Combination of Meropenem and Zinc Oxide Nanoparticles; Antimicrobial Synergism, Exaggerated Antibiofilm Activity, and Efficient Therapeutic Strategy against Bacterial Keratitis. *Antibiotics* **2022**, *11*, 1374. [CrossRef]
18. Ruden, S.; Hilpert, K.; Berditsch, M.; Wadhwani, P.; Ulrich, A.S. Synergistic interaction between silver nanoparticles and membrane-permeabilizing antimicrobial peptides. *Antimicrob. Agents Chemother.* **2009**, *53*, 3538–3540. [CrossRef]
19. Zhong, L.; Liu, H.; Samal, M.; Yun, K. Synthesis of ZnO nanoparticles-decorated spindle-shaped graphene oxide for application in synergistic antibacterial activity. *J. Photochem. Photobiol. B* **2018**, *183*, 293–301. [CrossRef]
20. Verma, S.K.; Jha, E.; Panda, P.K.; Das, J.K.; Thirumurugan, A.; Suar, M.; Parashar, S.K.S. Molecular aspects of core-shell intrinsic defect induced enhanced antibacterial activity of ZnO nanocrystals. *Nanomedicine* **2018**, *13*, 43–68. [CrossRef]
21. Bezza, F.A.; Tichapondwa, S.M.; Chirwa, E.M.N. Fabrication of monodispersed copper oxide nanoparticles with potential application as antimicrobial agents. *Sci. Rep.* **2020**, *10*, 16680. [CrossRef] [PubMed]
22. Huang, B.; Zhang, Y. Teaching an old dog new tricks: Drug discovery by repositioning natural products and their derivatives. *Drug Discov. Today* **2022**, *27*, 1936–1944. [CrossRef] [PubMed]
23. Nourbakhsh, F.; Lotfalizadeh, M.; Badpeyma, M.; Shakeri, A.; Soheili, V. From plants to antimicrobials: Natural products against bacterial membranes. *Phytother. Res.* **2022**, *36*, 33–52. [CrossRef] [PubMed]
24. Guzzo, F.; Scognamiglio, M.; Fiorentino, A.; Buommino, E.; D'Abrosca, B. Plant Derived Natural Products against *Pseudomonas aeruginosa* and *Staphylococcus aureus*: Antibiofilm Activity and Molecular Mechanisms. *Molecules* **2020**, *25*, 5024. [CrossRef] [PubMed]
25. Lee, J.H.; Kim, Y.G.; Yong Ryu, S.; Lee, J. Calcium-chelating alizarin and other anthraquinones inhibit biofilm formation and the hemolytic activity of *Staphylococcus aureus*. *Sci. Rep.* **2016**, *6*, 19267. [CrossRef]
26. Coenye, T.; Honraet, K.; Rigole, P.; Nadal Jimenez, P.; Nelis, H.J. In vitro inhibition of *Streptococcus mutans* biofilm formation on hydroxyapatite by subinhibitory concentrations of anthraquinones. *Antimicrob. Agents Chemother.* **2007**, *51*, 1541–1544. [CrossRef]
27. Nam, W.; Kim, S.P.; Nam, S.H.; Friedman, M. Structure-Antioxidative and Anti-Inflammatory Activity Relationships of Purpurin and Related Anthraquinones in Chemical and Cell Assays. *Molecules* **2017**, *22*, 265. [CrossRef]
28. Wei, Y.; Liu, Q.; Yu, J.; Feng, Q.; Zhao, L.; Song, H.; Wang, W. Antibacterial mode of action of 1,8-dihydroxy-anthraquinone from Porphyra haitanensis against *Staphylococcus aureus*. *Nat. Prod. Res.* **2015**, *29*, 976–979. [CrossRef]
29. Wang, J.; Qu, Q.; Liu, X.; Cui, W.; Yu, F.; Chen, X.; Xing, X.; Zhou, Y.; Yang, Y.; Bello-Onaghise, G.; et al. 1-Hydroxyanthraquinone exhibited antibacterial activity by regulating glutamine synthetase of *Staphylococcus xylosus* as a virulence factor. *Biomed. Pharmacother.* **2020**, *123*, 109779. [CrossRef]
30. Lee, J.H.; Kim, Y.G.; Park, S.; Hu, L.; Lee, J. Phytopigment Alizarin Inhibits Multispecies Biofilm Development by *Cutibacterium acnes*, *Staphylococcus aureus*, and *Candida albicans*. *Pharmaceutics* **2022**, *14*, 1047. [CrossRef]

31. Zhou, J.; Qi, G.B.; Wang, H. A purpurin-peptide derivative for selective killing of Gram-positive bacteria via insertion into cell membrane. *J. Mater. Chem. B* **2016**, *4*, 4855–4861. [CrossRef] [PubMed]
32. Song, Z.M.; Zhang, J.L.; Zhou, K.; Yue, L.M.; Zhang, Y.; Wang, C.Y.; Wang, K.L.; Xu, Y. Anthraquinones as Potential Antibiofilm Agents Against Methicillin-Resistant *Staphylococcus aureus*. *Front. Microbiol.* **2021**, *12*, 709826. [CrossRef] [PubMed]
33. Xiang, H.; Cao, F.; Ming, D.; Zheng, Y.; Dong, X.; Zhong, X.; Mu, D.; Li, B.; Zhong, L.; Cao, J.; et al. Aloe-emodin inhibits *Staphylococcus aureus* biofilms and extracellular protein production at the initial adhesion stage of biofilm development. *Appl. Microbiol. Biotechnol.* **2017**, *101*, 6671–6681. [CrossRef] [PubMed]
34. Dukanovic, S.; Ganic, T.; Loncarevic, B.; Cvetkovic, S.; Nikolic, B.; Tenji, D.; Randjelovic, D.; Mitic-Culafic, D. Elucidating the antibiofilm activity of Frangula emodin against *Staphylococcus aureus* biofilms. *J. Appl. Microbiol.* **2022**, *132*, 1840–1855. [CrossRef] [PubMed]
35. Park, B.S.; Kim, J.R.; Lee, S.E.; Kim, K.S.; Takeoka, G.R.; Ahn, Y.J.; Kim, J.H. Selective growth-inhibiting effects of compounds identified in *Tabebuia impetiginosa* inner bark on human intestinal bacteria. *J. Agric. Food Chem.* **2005**, *53*, 1152–1157. [CrossRef]
36. Yi, S.; Wu, Y.; Zhang, Y.; Zou, Y.; Dai, F.; Si, Y. Antibacterial Activity of Photoactive Silk Fibroin/Cellulose Acetate Blend Nanofibrous Membranes against *Escherichia coli*. *ACS Sustain. Chem. Eng.* **2020**, *8*, 16775–16780. [CrossRef]
37. Vanamala, K.; Tatiparti, K.; Bhise, K.; Sau, S.; Scheetz, M.H.; Rybak, M.J.; Andes, D.; Iyer, A.K. Novel approaches for the treatment of methicillin-resistant *Staphylococcus aureus*: Using nanoparticles to overcome multidrug resistance. *Drug Discov. Today* **2021**, *26*, 31–43. [CrossRef]
38. Bai, B.; Saranya, S.; Dheepaasri, V.; Muniasamy, S.; Alharbi, N.S.; Selvaraj, B.; Undal, V.S.; Gnanamangai, B.M. Biosynthesized copper oxide nanoparticles (CuO NPs) enhances the anti-biofilm efficacy against K. pneumoniae and S. aureus. *J. King Saud Univ. Sci.* **2022**, *34*, 102120. [CrossRef]
39. Naskar, A.; Cho, H.; Kim, K.S. A Nanocomposite with Extracellular Vesicles from Lactobacillus paracasei as a Bioinspired Nanoantibiotic Targeting *Staphylococcus aureus*. *Pharmaceutics* **2022**, *14*, 2273. [CrossRef]
40. Kumari, P.; Panda, P.K.; Jha, E.; Kumari, K.; Nisha, K.; Mallick, M.A.; Verma, S.K. Mechanistic insight to ROS and Apoptosis regulated cytotoxicity inferred by Green synthesized CuO nanoparticles from Calotropis gigantea to Embryonic Zebrafish. *Sci. Rep.* **2017**, *7*, 16284. [CrossRef]
41. Naskar, A.; Shin, J.; Kim, K.S. A MoS_2 based silver-doped ZnO nanocomposite and its antibacterial activity against beta-lactamase expressing *Escherichia coli*. *RSC Adv.* **2022**, *12*, 7268–7275. [CrossRef] [PubMed]
42. Kim, K.-S.; Kim, T.; Pan, J.G. In vitro evaluation of ciclopirox as an adjuvant for polymyxin B against gram-negative bacteria. *J. Antibiot.* **2015**, *68*, 395–398. [CrossRef] [PubMed]
43. Arul Selvaraj, R.C.; Rajendran, M.; Nagaiah, H.P. Re-Potentiation of beta-Lactam Antibiotic by Synergistic Combination with Biogenic Copper Oxide Nanocubes against Biofilm Forming Multidrug-Resistant Bacteria. *Molecules* **2019**, *24*, 3055. [CrossRef]
44. Caso Coelho, V.; Pereira Neves, S.D.; Cintra Giudice, M.; Benard, G.; Lopes, M.H.; Sato, P.K. Evaluation of antimicrobial susceptibility testing of Nocardia spp. isolates by broth microdilution with resazurin and spectrophotometry. *BMC Microbiol.* **2021**, *21*, 331. [CrossRef] [PubMed]
45. O'Toole, G.A. Microtiter dish biofilm formation assay. *J. Vis. Exp.* **2011**, 2437. [CrossRef]
46. Pham, D.T.N.; Khan, F.; Phan, T.T.V.; Park, S.K.; Manivasagan, P.; Oh, J.; Kim, Y.M. Biofilm inhibition, modulation of virulence and motility properties by FeOOH nanoparticle in *Pseudomonas aeruginosa*. *Braz. J. Microbiol.* **2019**, *50*, 791–805. [CrossRef]
47. Shin, J.; Naskar, A.; Ko, D.; Kim, S.; Kim, K.-S. Bioconjugated Thymol-Zinc Oxide Nanocomposite as a Selective and Biocompatible Antibacterial Agent against *Staphylococcus* Species. *Int. J. Mol. Sci.* **2022**, *23*, 6770. [CrossRef]
48. Shin, J.; Magar, K.B.S.; Lee, J.; Kim, K.-S.; Lee, Y.R. Design, synthesis, and discovery of novel oxindoles bearing 3-heterocycles as species-specific and combinatorial agents in eradicating *Staphylococcus* species. *Sci. Rep.* **2019**, *9*, 8012. [CrossRef]
49. Cheng, G.; Hight Walker, A.R. Transmission electron microscopy characterization of colloidal copper nanoparticles and their chemical reactivity. *Anal. Bioanal. Chem.* **2010**, *396*, 1057–1069. [CrossRef]
50. Ingle, A.P.; Rai, M. Copper nanoflowers as effective antifungal agents for plant pathogenic fungi. *IET Nanobiotechnol.* **2017**, *11*, 546–551. [CrossRef]
51. Nicolae Dopcea, G.; Dopcea, I.; Nanu, A.E.; Diguta, C.F.; Matei, F. Resistance and cross-resistance in *Staphylococcus* spp. strains following prolonged exposure to different antiseptics. *J. Glob. Antimicrob. Resist.* **2020**, *21*, 399–404. [CrossRef] [PubMed]
52. Brown, M.M.; Horswill, A.R. *Staphylococcus epidermidis*-Skin friend or foe? *PLoS Pathog.* **2020**, *16*, e1009026. [CrossRef]
53. Byrd, A.L.; Deming, C.; Cassidy, S.K.B.; Harrison, O.J.; Ng, W.I.; Conlan, S.; Program, N.C.S.; Belkaid, Y.; Segre, J.A.; Kong, H.H. *Staphylococcus aureus* and *Staphylococcus epidermidis* strain diversity underlying pediatric atopic dermatitis. *Sci. Transl. Med.* **2017**, *9*, eaal4651. [CrossRef] [PubMed]
54. Jena, S.; Panda, S.; Nayak, K.C.; Singh, D.V. Identification of Major Sequence Types among Multidrug-Resistant Staphylococcus epidermidis Strains Isolated from Infected Eyes and Healthy Conjunctiva. *Front. Microbiol.* **2017**, *8*, 1430. [CrossRef]
55. Hiltunen, A.K.; Savijoki, K.; Nyman, T.A.; Miettinen, I.; Ihalainen, P.; Peltonen, J.; Fallarero, A. Structural and Functional Dynamics of *Staphylococcus aureus* Biofilms and Biofilm Matrix Proteins on Different Clinical Materials. *Microorganisms* **2019**, *7*, 584. [CrossRef]
56. Schilcher, K.; Horswill, A.R. Staphylococcal biofilm development: Structure, regulation, and treatment strategies. *Microbiol. Mol. Biol. Rev.* **2020**, *84*, e00026-19. [CrossRef]
57. Rajamohan, R.; Raorane, C.J.; Kim, S.C.; Lee, Y.R. One Pot Synthesis of Copper Oxide Nanoparticles for Efficient Antibacterial Activity. *Materials* **2022**, *16*, 217. [CrossRef]

58. Dell'Annunziata, F.; Folliero, V.; Palma, F.; Crudele, V.; Finamore, E.; Sanna, G.; Manzin, A.; De Filippis, A.; Galdiero, M.; Franci, G. Anthraquinone Rhein Exhibits Antibacterial Activity against *Staphylococcus aureus*. *Appl. Sci.* **2022**, *12*, 8691. [CrossRef]
59. Cruz, C.D.; Shah, S.; Tammela, P. Defining conditions for biofilm inhibition and eradication assays for Gram-positive clinical reference strains. *BMC Microbiol.* **2018**, *18*, 173. [CrossRef]
60. Ravikumar, V.; Mijakovic, I.; Pandit, S. Antimicrobial Activity of Graphene Oxide Contributes to Alteration of Key Stress-Related and Membrane Bound Proteins. *Int. J. Nanomed.* **2022**, *17*, 6707–6721. [CrossRef]
61. Lebre, P.H.; De Maayer, P.; Cowan, D.A. Xerotolerant bacteria: Surviving through a dry spell. *Nat. Rev. Microbiol.* **2017**, *15*, 285–296. [CrossRef] [PubMed]
62. Kornder, J.D. Streptomycin revisited: Molecular action in the microbial cell. *Med. Hypotheses* **2002**, *58*, 34–46. [CrossRef] [PubMed]
63. Aguirre Rivera, J.; Larsson, J.; Volkov, I.L.; Seefeldt, A.C.; Sanyal, S.; Johansson, M. Real-time measurements of aminoglycoside effects on protein synthesis in live cells. *Proc. Natl. Acad. Sci. USA* **2021**, *118*, e2013315118. [CrossRef] [PubMed]